Beach-face slope dataset for Australia

Kilian Vos[1], Wen Deng[1], Mitchell D. Harley[1], Ian L. Turner[1], Kristen D. Splinter[1]

[1]Water Research Laboratory, School of Civil and Environmental Engineering, UNSW Sydney, 110 King Street, Manly Vale, NSW 2093, Australia

5   *Correspondence to*: Kilian Vos (k.vos@unsw.edu.au)

Abstract. Sandy beaches are unique environments composed of unconsolidated sediments that are constantly reshaped by the action of waves, tides, currents, and winds. The most seaward region of the dry beach, referred to as the beach face, is the primary interface between land and ocean and is of fundamental importance to coastal processes, including the dissipation and reflection of wave energy at the coast, and the exchange of sediment between the land and sea. The slope of the beach-face is a critical parameter in coastal geomorphology and coastal engineering, necessary

10   to calculate the total elevation and excursion of wave run-up at the shoreline. However, datasets of the beach-face slope remain unavailable along most of the world's coastlines. This study presents a new dataset of beach-face slopes for the Australian coastline derived from a novel remote sensing technique. The dataset covers 13,200 km of sandy coast and provides an estimate of the beach-face slope at every 100 m alongshore, accompanied by an easy to apply measure of the confidence of each slope estimate. The dataset offers a unique view of large-scale spatial variability in beach-face slope and addresses the growing need for this information to predict coastal hazards around Australia. The beach-face slope dataset

15   and relevant metadata are available at https://doi.org/10.5281/zenodo.5606217 (Vos et al., 2021).

1 Introduction

The world's coastlines are unique geological environments at the interface between land and sea. Along this coastal fringe, which is often densely populated (Small et al., 2011), we find beaches composed of unconsolidated sediments (e.g., gravel, sand, mud) that are constantly reshaped by the action of waves, currents, winds and tides (Dean and Dalrymple, 2004). A typical beach cross-section, or beach profile, is illustrated in Figure 1.

20   The beach face is the most seaward region of the subaerial beach, which extends from the berm to the low tide water line and is constantly interacting with the uprush and downrush of individual waves and tidal cycles. The steepness of the beach face (tanβ), or beach-face slope, is a key parameter in coastal geomorphology and coastal engineering due to its control on important coastal processes. Crucially, the beach-face slope controls the elevation of wave run-up and total swash excursion at the shoreline (Gomes da Silva et al., 2020; Stockdon et al., 2006), processes that are of primary importance for the assessment of coastal erosion and inundation hazards along the coastal boundary (Senechal et al., 2011; Stockdon et

25   al., 2007). The beach-face slope parameter is also a useful proxy for surf-zone hydrodynamics in the absence of costly surf-zone bathymetric surveys and can provide insights into beach swimmer safety (Short et al., 1993) and wave set-up across the surf zone (Stephens et al., 2011).

Despite the importance of the beach-face slope parameter in numerous empirical formulations in coastal engineering (e.g., wave run-up prediction), large-scale datasets of the beach-face slope remain unavailable along most of the world's coastlines. A complementary global dataset of nearshore slopes, defined from Mean Sea Level (MSL) to the 'closure depth' where negligible morphological change theoretically occurs, was recently compiled by Athanasiou et al. (2019). Referring to Figure 1, this slope indicates the cross-shore gradient of the subaqueous (below MSL) profile and is generally much lower in gradient than the beach-face slope.

The steepness of the beach face is closely related to grain size (Bujan et al., 2019), with coarser (finer) sediment typically adopting a steeper (flatter) beach face, however it is also linked to the morphodynamic beach state, with lower-gradient slopes usually found along high-energy dissipative beaches and steeper slopes along low-energy reflective beaches (Wright and Short, 1984). The beach-face slope can be measured by using survey techniques such as topographic RTK-GPS measurements, but these methods require human intervention and remain impractical over large spatial scales (regional to continental). In recent decades, Airborne LiDAR technology has significantly increased the spatial coverage of coastal topographic data, from individual beaches to hundreds of kilometres of coastline (e.g., Middleton et al., 2013; Stockdon et al., 2002). However, in the swash zone, these active remote sensing techniques are hampered by the constant alternating of wet and dry phases as water levels fluctuate at the shoreline under the action of waves and tides slopes (Middleton et al., 2013), limiting the ability to extract beach-face slopes. UAV surveys and aerial photogrammetry are also subject to the same caveat as structure-from-motion techniques fail in the swash zone due to the non-stationary ground target (Pucino et al., 2021; Turner et al., 2016). More recently, novel methods to extract intertidal zone information using publicly available optical imagery and tide models have been developed (Bishop-Taylor et al., 2019; Tseng et al., 2017), considerably increasing our ability to map coastal topography over large spatial scales. Recently, Vos et al. (2020) introduced a method to specifically estimate the beach-face slope combining instantaneous satellite-derived shorelines with predicted tides and capable of accurately estimating the long-term average slope between MSL and Mean High Water Springs (MHWS), the region highlighted in Figure 1, across a wide range of coastal environments. This new method paves the way for the generation of large-scale beach-face slope datasets to complement the present nearshore slope global dataset and better resolve the coastal topography.

In Australia, a national dataset of coastal topography and bathymetry was recently identified by the marine research, industry and stakeholder communities as a key priority to improve the ability to model hazards associated with waves and storm surge (Greenslade et al., 2020). More specifically, O'Grady et al. (2019) investigated the contribution of wind waves to total water levels along the Australian coastline and concluded that a key limitation for an accurate operational coastal inundation forecasting system was the lack of a continental-scale beach-face slope dataset. Historically, due to there being no alternative, studies that have focused on continental to regional scales have adopted uniform beach-face slope values. For example, recent studies investigating the contribution of wave processes to relative sea-level-rise have either used slope-independent

runup formulations (Vitousek et al., 2017) or opted for a constant and therefore arbitrary beach-face slope of 0.1 for all of the world's coastlines (Melet et al., 2018) which has attracted criticism of this approach (Aucan et al., 2019).

In this contribution, we use a recently published and validated beach-face slope estimation technique (Vos et al., 2020) to fill this gap for the Australian continent. We present a new dataset of beach-face slopes spaced at 100 m increments alongshore for every sandy beach in Australia totalling 13,200 km of sandy coastline. Each beach-face slope estimate is based on the average slope over the past 20 years and is associated with an easy-to-apply measure of confidence. The methodology to estimate beach-face slopes and confidence bands is presented in the next section. A synopsis then follows of the large-scale spatial variability in beach-face slopes around the Australian continent, and the integration of this dataset with the National Sediment Compartment Framework for Australia (Thom et al., 2018). The paper concludes with a brief section illustrating potential use cases of this new dataset for coastal management and flood risk modelling studies.
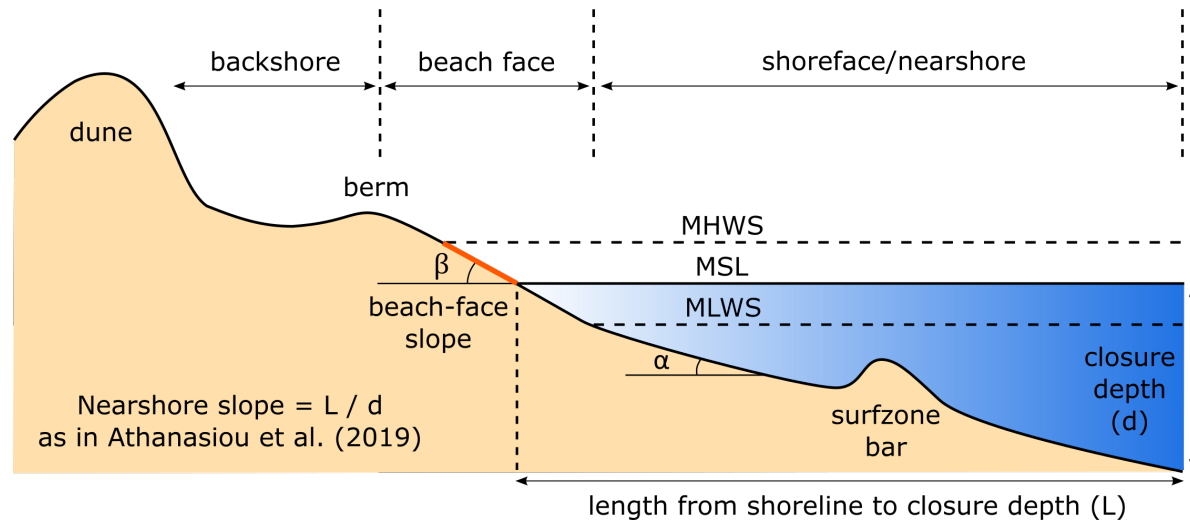
Figure 1. Schematic of a beach profile from the dune to the depth of closure, adapted from Coastal Engineering Research Center (1984). The beach-face slope (tanβ) that is mapped in this work is a proxy for the slope of the portion of the profile that is highlighted in orange, extending from Mean Sea Level (MSL) up to Mean High Water Spring (MHWS). The beach-face slope complements the global dataset of nearshore slopes presented in Athanasiou et al. (2019) that represents the slope extending from the depth of closure up to MSL.

2 Methods

2.1 Transects dataset

A dataset of shore-normal transects along the Australian sandy coastline was created semi-automatically. Sandy beaches were first extracted from the OpenStreetMaps database (OSM, 2017) and manually quality-controlled in a GIS environment (QGIS Development Team, 2021). In total, 5,207 sandy beaches were identified along open coasts and semi-enclosed regions. The sandy shoreline locations were then used to generate 100 m alongshore-spaced cross-shore transects with the "*v_transects*" functionality of GRASS GIS (GRASS Development Team, 2020), generating a total of 132,000 individual transects extending along 13,200 km of sandy coastline circumnavigating the Australian continent. The beach-face slope was estimated along each transect as described in the following section.

2.2 Beach-face slope estimation algorithm

A novel remote sensing technique to estimate beach-face slopes from satellite imagery and modelled tides was applied to each of the 132,000 sandy beach transects. This method, described in detail in Vos et al. (2020), combines 20-year time-series of shoreline change derived from Landsat imagery with tidal predictions at the time of image acquisition to estimate the slope of the beach face. Briefly, the concept behind this method is that instantaneous shoreline time-series, mapped on images that were acquired at different stages of the tide, contain a tidal signal that is modulated by the beach-face slope and can be isolated in the frequency domain due to its periodicity. Thus, this technique uses the frequency domain and iteratively seeks a value of the slope that minimises the tidal energy when used for tidal correction. Tidal correction consists of the projection of individual instantaneous shorelines, acquired at different stages of the tide, to a standard reference elevation such as MSL. A simple tidal correction is then applied by translating horizontally the shoreline points along a cross-shore transect using a linear slope:

$$\Delta x_{corrected} = \Delta x + \frac{z_{tide}}{tan\beta} \tag{1}$$

where $\Delta x_{corrected}$ is the tidally-corrected cross-shore position, Δx is the instantaneous cross-shore position, z_{tide} is the corresponding tide level and $tan\beta$ is the beach-face slope.

The first step is to map instantaneous shorelines spanning a full 20 years of all available Landsat imagery (Landsat 5, 7 and 8) at every sandy beach and then determine the intersection of individual shorelines with each of the 100 m spaced transects to obtain time-series of (non-tidally corrected) shoreline change, an example of this is shown in Figure 2a for Cable Beach, Western Australia. Time-series are obtained with CoastSat, a toolbox publicly available at https://github.com/kvos/CoastSat and described in Vos et al., (2019). The 20-year time period (1999-2020) is selected to ensure

that two Landsat satellites are in orbit simultaneously, which theoretically results in a combined revisit period of 8 days (16 days for each satellite). However, in practice, time-series of shoreline change are irregularly sampled due to factors such as cloud cover, gaps in Landsat 7 data (scan line corrector error) and discarded images due to poor geometric or radiometric quality. Any outliers in the shoreline time-series (e.g., due to false detections) are also removed using a despiking algorithm.

Next, tide levels associated with every shoreline observation are extracted from the global tide model FES2014 (Carrere et al., 2016), as shown in Figure 2b. The tide level time-series are then transformed to frequency domain, and since these are not evenly sampled, an alternative to the Fourier transform, the Lomb-Scargle transform (Lomb, 1976; VanderPlas, 2018) is employed to compute the power spectrum density (PSD). Since the Lomb-Scargle is a least-squares spectral method, the limits and spacing of the frequency grid need to be first defined. Here, a main sampling period of 8 days (i.e., the theoretical Landsat revisit period) is used, resulting in a maximum frequency (Nyquist limit) of 16 days, and the spacing n_0 is set to 50 samples per peak to ensure that the grid sufficiently samples each peak (VanderPlas, 2018, Section 7.1). In the resulting PSD, the frequency with the highest peak is isolated, which corresponds to the frequency where the tidal signal (e.g., the spring-neap tidal cycle) is strongest in the sub-sampled time-series and is referred to as the 'peak tidal frequency'. Note that the spring-neap cycle has a period of 14.8 days but is subject to aliasing when sampled at an 8-day interval resulting in a peak at 17.5 days (refer Supporting Information S3 in Vos et al., 2020).

The final steps in obtaining the time-averaged estimate of the beach-face slope at every 100 m alongshore consists of tidally-correcting the time-series of raw shoreline change across an iterative range of slope values from 0.01 to 0.2 (following the range identified in Bujan et al., 2019). For each slope value, the tidally-corrected time-series is transformed to the frequency domain and, by integrating each PSD inside the peak tidal frequency band, a curve of tidal energy vs slope is constructed (Figure 2c). The best estimate of the beach-face slope is then the value that minimises this tidal energy in the peak tidal frequency band (Figure 2d). A full example of this procedure is presented for both a microtidal site (Narrabeen-Collaroy) and a macrotidal site (Cable Beach) in the form of Jupyter notebooks at https://github.com/kvos/CoastSat.slope (Vos, 2021b).

This beach-face slope estimation technique was validated against *in situ* (beach survey) data along 8 diverse sandy/gravel beaches spanning a broad range of beach-face slopes, tidal regimes, and wave climates (Vos et al., 2020). The validation sites — namely Narrabeen-Collaroy, Moruya-Pedro and Cable Beach in Australia, Duck and Torrey Pines in the USA, Slapton Sands UK, Tairua Beach NZ, and Ensenada MEX — range from microtidal wave-dominated to macrotidal tide-modified beaches, with the *in situ* measured average beach-face slopes varying from tanβ = 0.025 to tanβ = 0.14. The satellite-derived beach-face slope estimates were found to match best with the slope between MSL to MHWS (R^2 = 0.93, bias = 0.0), while they tended to overestimate the full intertidal (MLWS to MHWS) slope. This can be explained by the fact that the upper intertidal slope (MSL to MHWS) is generally more stable over time, while the lower intertidal slope (MLWS to MSL) is more variable as intertidal bars attach/detach to the shoreline (Wright and Short, 1984). Wave runup and setup effects that are not included in the global tide model also tend to skew the shoreline detection towards the upper part of the intertidal profile (e.g., Harley et al., 2019).

1999 ——————————————————→ 2021

CoastSat toolbox

Non-tidally-corrected time-series of shoreline change

Associated predicted tide levels from FES2014 model

Tidal correction with a range of slopes (+ tide levels / tanβ)

Peak tidal frequency (Lomb-Scargle transform)

Power Spectrum of tidally-corrected time-series at peak tidal frequency

17.5 days (peak tidal frequency)

values of tanβ   0.01   0.05   0.1   0.15   0.2

Integrate PSD inside peak tidal frequency band

Choose slope that minimises the tidal energy

min(E)

120

Figure 2. Flowchart of the methodology to estimate beach-face slopes from satellite-derived shorelines and predicted tides described in Vos et al. (2020). Firstly, instantaneous shorelines are mapped on Landsat imagery with the CoastSat toolbox. The time-series of non-tidally corrected shoreline change (a) and their associated tide levels (b) are then combined in frequency domain to find the slope that, when used for tidal correction, minimises the tidal signal. (c) shows the power spectrum density (PSD) of the tidally-corrected time-series, demonstrating how the slope value modulates the energy inside the tidal frequency band, plotted as a function of slope in (d).

125

2.3 Beach-face slope confidence bands

The tidal energy vs beach-face slope curve shown in Figure 2d is used to quantify the uncertainty of each beach-face slope estimate. When the minimum is very well defined in the curve (as in Figure 2d), this indicates high confidence in the estimate as there is a single value of the slope that clearly minimises the amount of energy in the peak tidal frequency band. However, at other locations, the minimum of the curve is not so well

130   defined, and several beach-face slope values correspond to similar levels of PSD energy, as shown in Figure 3 (from Narrabeen-Collaroy beach located in Sydney, NSW). To incorporate a simple-to-apply measure of uncertainty in the dataset of beach-face slope estimates, a 5% vertical band above the minimum amount of energy in the curve is used to estimate confidence bands around the slope estimate. To illustrate, Figure 3 shows the 5% band above the minimum energy, the slope that minimises the energy (0.075), and the lower bound (0.065) and upper bound (0.095) slopes that define the 5% of the minimum PSD energy. Note that given the shape of the energy vs beach-face slope curves, which generally tends to start as a

135   parabola and then flatten with an inflection point after the minimum, the confidence bands are not symmetric. While these are not 95% confidence intervals in the statistical sense, they provide practical information for end-users about the uncertainty associated with any individual slope estimate.
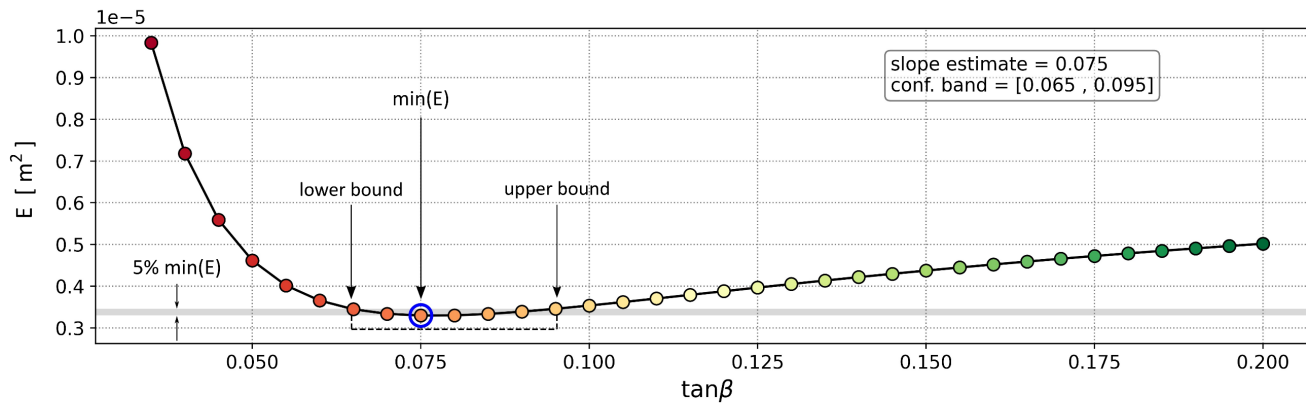
Figure 3. Estimation of confidence bands around each beach-face slope estimate based on the tidal energy vs slope curve. The lower and upper bounds are the slopes that are associated with a tidal energy within 5% of the minimum.

140 **3 Results**

3.1 Synopsis of the distribution of beach-face slopes around Australia

Beach-face slopes were estimated at each of the 132,000 beach transects, corresponding to 13,200 km of sandy coastline around Australia. The beach-face slope data was summarised from the transect scale to the individual beach scale by calculating the weighted average of all the transects at each beach, weighted by the width of the confidence bands to emphasise slopes with higher confidence. The resulting average beach-face slope

145 for every sandy beach around the continent is presented in Figure 4a. Beach-face slope values range between 0.01 and 0.18. The distribution of beach-face slopes for each of the 7 coastal states in Australia is shown in Figure 4b, indicating median values between 0.055 (Victoria) and 0.08 (Northern Territory), with all 7 interquartile ranges sitting between 0.045 and 0.11.

Along the wave-dominated and energetic southern half of Australia (refer Supplementary Figure 1b), the dataset shows very low gradient beaches (0.01-0.035) along the western coast of Tasmania, western Victoria, and south-west WA. Large spatial variability in beach-face slopes is observed

150 along the tide-modified/tide-dominated northern half of Australia, with Queensland showing the widest interquartile range (from 0.05 to 0.11).
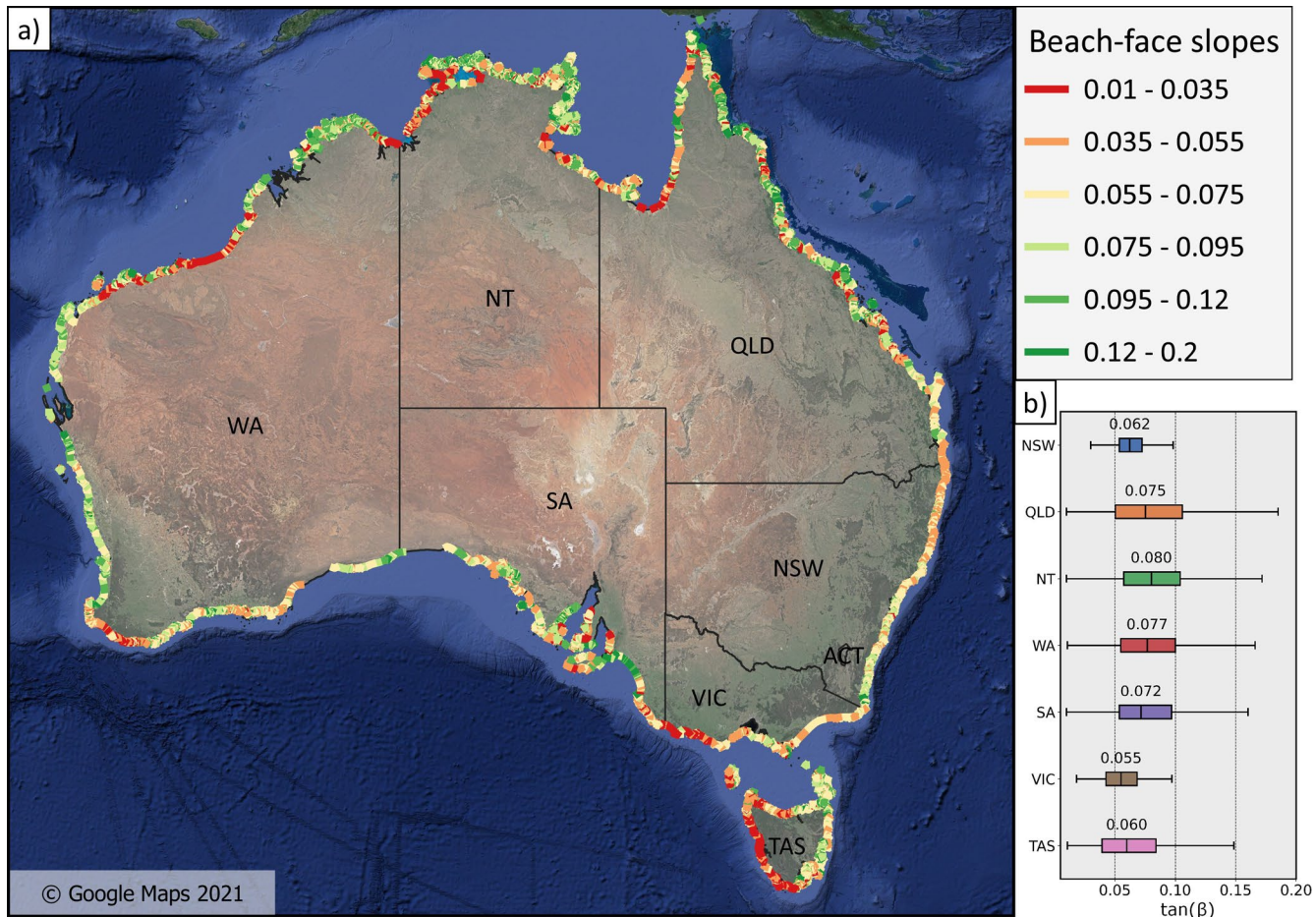
Figure 4. Beach-face slopes around Australia along 132,000 100m-spaced transects (equivalent to 13,200 km of coast). (b) shows the distribution for each Australian state.

While State administrative boundaries provide a first division of the country, useful for high-level management purposes, they are not representative
155   of the geology, surface landforms and shoreline orientation of the Australian coastline. To address this, Thom et al. (2018) proposed a national
sediment compartment framework that provides a hierarchical division of the coast integrating inshore/offshore geological factors, major structural
landforms such as headlands and changes in shoreline orientation. On this basis, the Australian continent is divided into 23 coastal 'regions', 100
'primary sediment compartments' and 361 'secondary sediment compartments'. The beach-face slope distribution (weighted-average per beach)
for each of the 23 coastal regions is presented in Figure 5. Along the south-eastern coast, narrow slope distributions are observed in Central East

160 (2), Southern NSW (1) and Gippsland (20). Moving northwards, very wide distributions are observed in Central Queensland (3), Eastern (4) and Western Cape York Peninsula (5), and Southern Gulf of Carpentaria (6). The Northern Territory (NT) shows a clear contrast between the relatively steep beaches of East and North Arnhem Land (7-8) and the extremely low gradient Western NT (9). A similar distinction is observed in the northern part of Western Australia (WA), where the manifold of islands in the Kimberley region (10) show steep slopes that contrast with the long and low gradient beaches of the Pilbara region (11). As the tide-modified/tide-dominated coast transitions to wave-dominated, a gradient of

165 decreasing beach-face slopes is observed along the western regions of Central West WA (12), Southwest WA (13) and Southern WA (14). Wide beach-face slope distributions are observed in South Australia (SA), regions 15-18, which comprises long microtidal coasts, mesotidal gulfs and large offshore islands. The remaining region of the continental mainland is Central and Western Victoria (19), which contains relatively low gradient beaches (median of 0.05). Finally, in Tasmania a clear distinction between the intermediate slopes of the North (21) and East coasts (22) and the West (23) coast is apparent, noting that West Tasmania exhibits the lowest beach-face slopes (median 0.03) of all the coastal regions around

170 Australia.
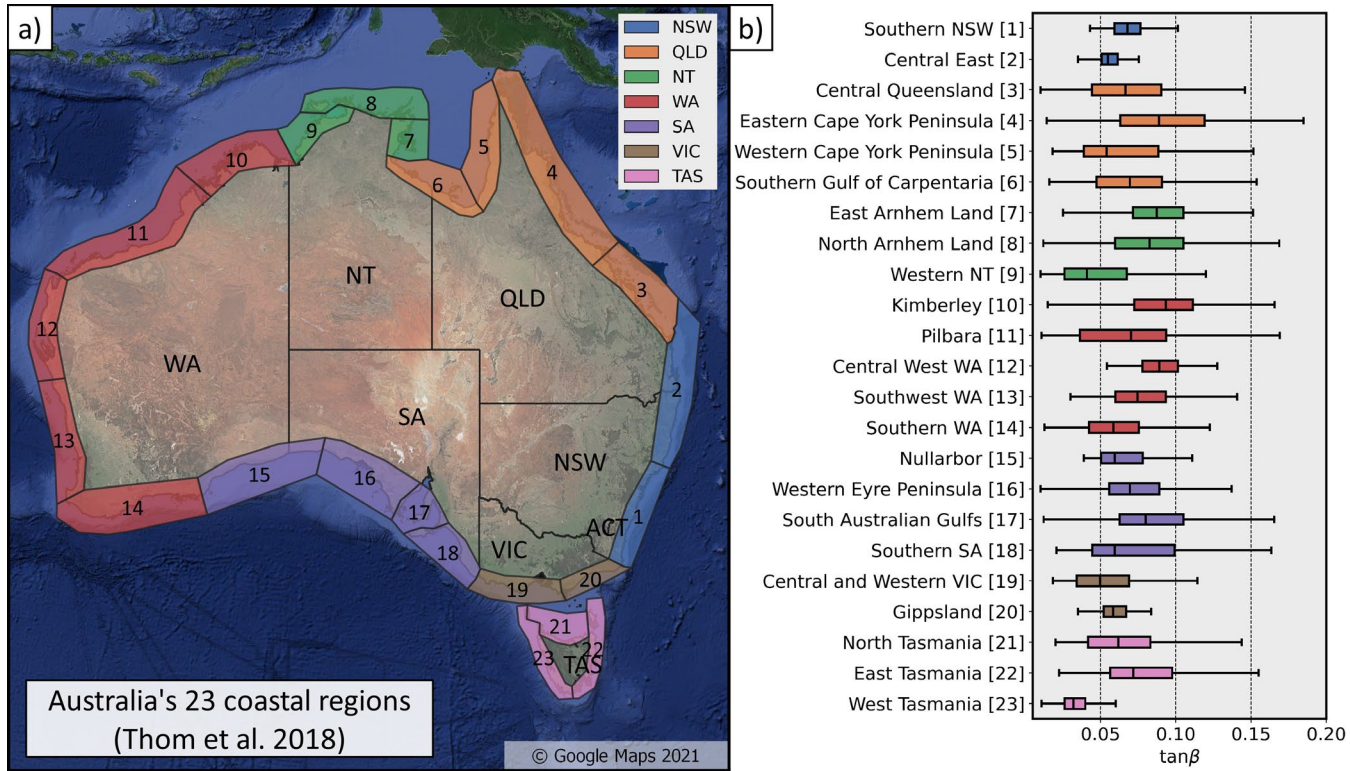
Figure 5. Distribution of beach-face slopes for each of the 23 coastal regions identified by Thom et al. (2018).

The widths of the corresponding beach-face slope confidence bands, described in Section 2.3 provide a simple-to-apply metric and filter on the uncertainty in slope estimates. Figure 6a presents a map of the beach-averaged width of the confidence bands, color-coded with a simple three-category 'traffic-light' system: *high confidence* (green) when below 0.025, *medium confidence* (yellow) between 0.025 and 0.05 and *low confidence* (red) above 0.05. Using these categories, 56% of the continental-scale dataset indicate *high confidence*, with 23% *medium confidence* and 21% *low confidence*. Figure 6b shows the distribution of this confidence metric across each of the 23 regions. Extensive areas of low confidence are observed along the west and south coasts of WA and most of SA, while the remainder of the coastline generally indicates high confidence, interspersed by isolated occurrences of low/medium confidence (e.g., east Arnhem Land, south-east Tasmania). The median width of confidence bands is below 0.025 (i.e., high confidence) for 13 of the 23 coastal regions, between 0.025 and 0.5 (medium confidence) for 5 regions (East Arnhem Land, Central West WA, Western Eyre Peninsula, East/West Tasmania) and above 0.5 (low confidence) for 5 regions including south-west and southern WA and the majority of SA.
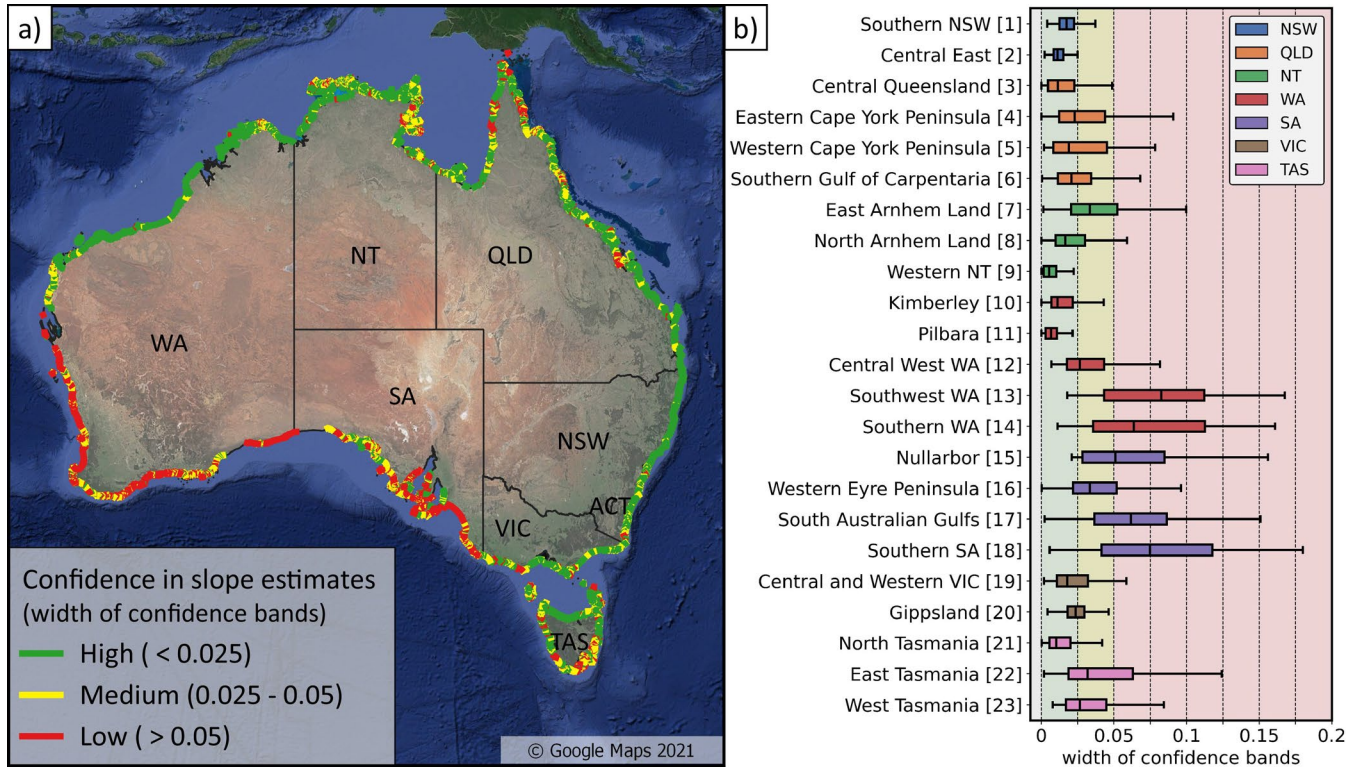
Figure 6. Traffic-light system indicating the uncertainty in the beach-face slope estimates. (b) shows the distribution of the width of confidence bands across the 23 regions, indicating on average high confidence across 13 regions, medium confidence across 5 regions (7,12,16,22,23) and low confidence across 5 regions (13,14,15,17,18).

Vos et al. (2020) previously identified that the performance of the beach-face slope estimation method depends on the signal-to-noise ratio between the accuracy of the satellite-derived shorelines (10-15m based on the validation in Vos et al. (2019b)) and the horizontal extent of the tidal excursion. Thus, the observation of greater uncertainty in slope estimates along south-west and south WA regions is consistent with the very small tidal range along this coast (< 1 m Mean Spring Tidal Range, see Supplementary Figure 1a). Another issue affecting the signal-to-noise ratio is the aliasing of the tidal signal by sun-synchronous sensors (i.e., Landsat orbits), which implies that the full tidal range may not always be captured by the satellite imagery (Bishop-Taylor et al., 2019; Eleveld et al., 2014). Figure 7 shows the percentage of the Mean Spring Tidal Range (MSTR) that is observed by the satellite-derived shorelines at each beach. This analysis reveals that the SA coastal regions (15-18), which exhibit lower confidence in Figure 6, have the lowest tide range coverage with only about 60-65% of the MSTR sampled (Figure 7a). Thus, along the SA regions which are already

microtidal (except inside the gulfs), this aliasing results in only part of the tidal range being observed in the available satellite imagery, further reducing the signal-to-noise ratio and leading to lower confidence slope estimates.
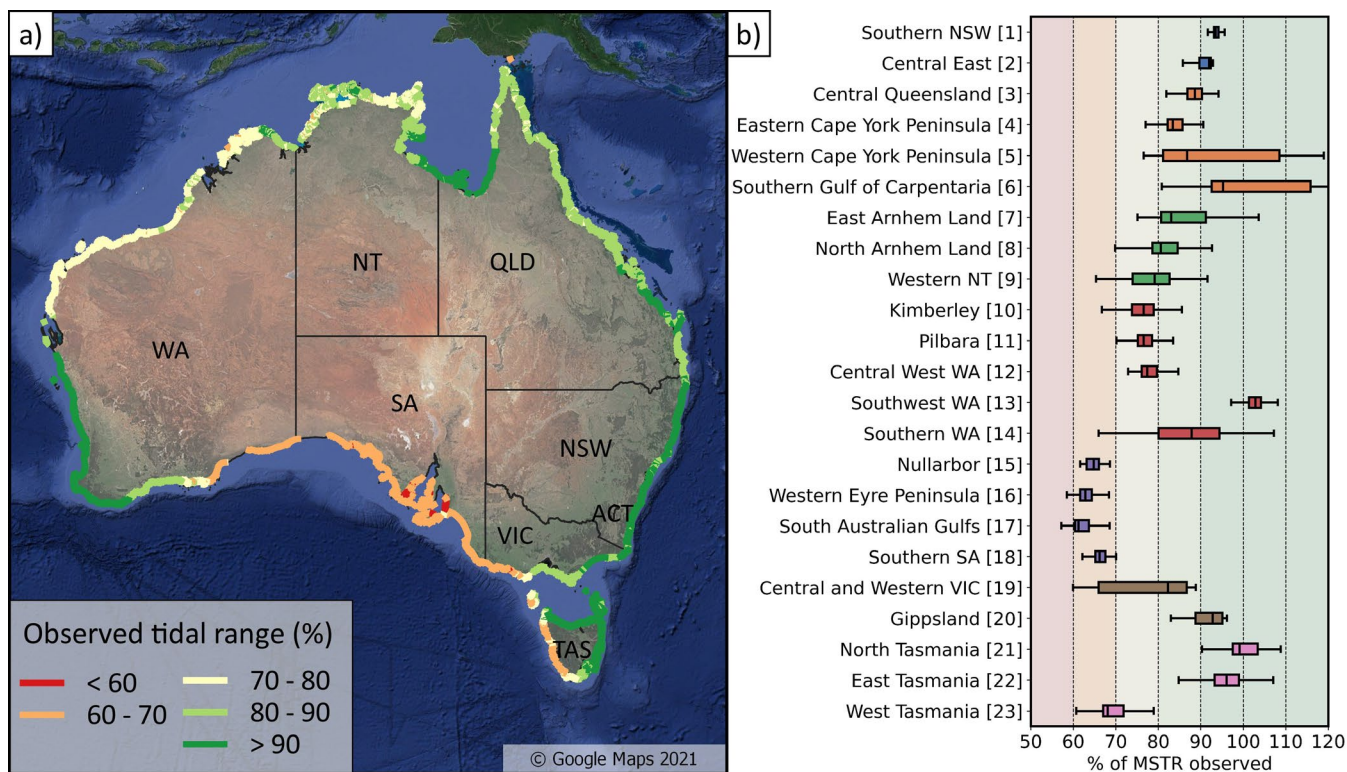
Figure 7. Observed tidal range by the satellite-derived shorelines. (a) maps the % of the MSTR that is observed at each beach and (b) shows the distribution of that metric across the 23 coastal regions.

3.2 An example embayment-scale application

While the previous section focused on the large-scale distribution of beach-face slopes at the continental scale, this dataset can also provide insights into variations in beach-face slope along any individual embayment or beach. To illustrate, Figure 8a shows beach-face slopes at the transect-scale (100 m spacing alongshore) along a single embayment, the Stockton Bight, located in NSW about 150 km north of Sydney. Stockton Bight is the longest beach in NSW, featuring 32-km of south-facing sandy coast backed by a large transgressive dune system (Short, 2020). The beach-face slope data at this site, shown in Figure 8a, indicates a distinct alongshore gradient, with lower gradient slopes towards the northern end of the

embayment (tanβ = 0.04) and steeper slopes in the southern (tanβ = 0.1). Interestingly, a sediment grain size dataset at this same site is reported by Pucino (2015), with the median swash zone sand size (D_{50}) at 20 equally spaced sample locations (Figure 8b) indicating a distinct gradient in grain size along the Stockton Bight embayment. The observed correlation between grain size and beach-face slope that is apparent in Figure 8 is in agreement with our understanding of this relationship, generally described by a power-law (Bujan et al., 2019). This example demonstrates that this

210 continental-wide dataset can also be utilised to gain insights into the alongshore variability of beach-face slopes (and, potentially, grain size distribution) along individual beaches and embayments, and inform present-day coastal management and planning.
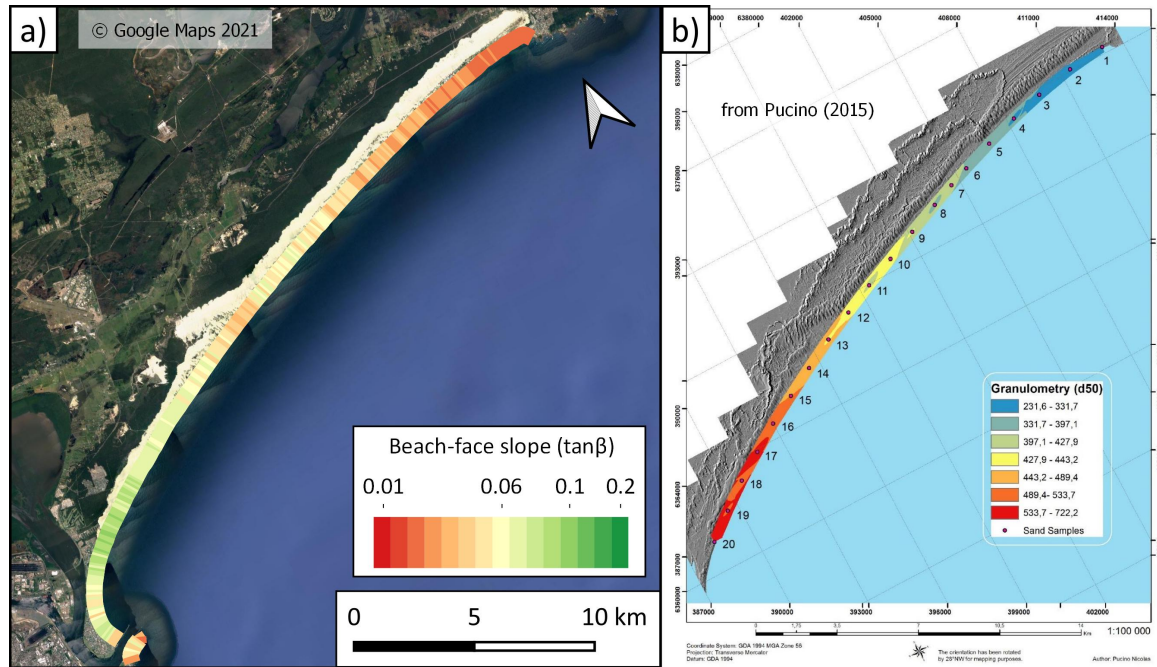
Figure 8. Embayment-scale gradient in beach-face slopes and sediment grain size. a) Beach-face slope estimates along 100-m spaced cross-shore transects along the Stockton Bight embayment. b) Figure taken from Pucino (2015) displaying the spatial distribution of median grain size (D_{50}) for 20 sand samples along the

215 embayment. D_{50} values are in microns and have been interpolated using inverse-weighted-distance and discretised into 7 quantiles.

3.3 Dataset description

The data presented above is made available as two geospatial layers (GeoJSON files): one providing the beach-face slope estimates on a transect basis (100 m alongshore spacing) and the second providing the estimates averaged over each individual beach. Tables 1 and 2 describe the attributes of each layer, respectively.

At the transect scale (Table 1), the beach-face slope and confidence bands are accompanied by relevant metadata such as the number of shoreline points used to estimate the beach-face slope, the sediment compartment/region in which the transect is located and a database ID for the transect. A confidence flag (high/medium/low) is associated with each estimate as is illustrated in Figure 6.

At the beach scale (Table 2), the alongshore-averaged slope weighted by the width of the confidence intervals is provided for each individual beach, associated with a confidence flag (high/medium/low) based on the alongshore-averaged width of the confidence bands. Relevant metadata at the beach scale include the Mean Spring Tide Range (MSTR), Median Significant Wave Height (Hsig), percentage of observed tide range, minimum observed tide level, maximum observed tide level and beach length.

To assist users of Australia's national sediment compartment framework (Figure 5), the distribution of beach-face slopes in each sediment compartment is provided in Supplementary Information at both the primary (Supplementary Figure 3) and secondary (Supplementary Figure 4) levels. Geospatial layers containing the primary and secondary compartments are also included in the dataset and displayed in Supplementary Figure 2.

Table 1. Description of data fields for the beach-face slope dataset at the transect scale

Attributes	Values	Description
transect_id	e.g., aus0001-0000, aus0001-0001, ...	Database id for each transect
beach_id	e.g., aus0001, aus0002, …, aus5255	Database id for each beach
beach_slope (tanβ)	$0.01 \leq x \leq 0.2$	Estimate of the beach-face slope (between MSL and MHWS)
lower_conf_bound	$0.01 \leq x \leq 0.2$	Lower limit of the confidence band
upper_conf_bound	$0.01 \leq x \leq 0.2$	Upper limit of the confidence band
width_conf_bound	$0 \leq x \leq 0.19$	Width of confidence band
sl_points	$100 \leq x \leq 1300$	Number of datapoints in the time-series used for beach-face slope estimation.
quality_flag	High / Medium / Low	Quality flag indicating the confidence in the slope estimate at this transect
coastal_region	e.g., Southern NSW, Central Queensland, …	Database id corresponding to the 23 coastal regions as identified by Thom et al. (2018)
primary_comp_id	e.g., NSW01.01, NSW01.02, QLD01.01, …	Database id corresponding to the 100 primary sediment compartments as identified by Thom et al. (2018)
secondary_comp_id	e.g., NSW01.01.01, NSW01.01.02, QLD01.01.01, QLD01.01.02, …	Database id corresponding to the 361 secondary sediment Compartments as identified by Thom et al. (2018)

235

Table 2. Description of data fields for the beach-face slope dataset at the individual beach scale

Attributes	Values	Description
beach_id	e.g., aus0001, aus0002, …, aus5255	Database id for each beach
beach_slope_average $(\overline{tan\beta})$	$0.01 \leq x \leq 0.2$	Average of the beach-face slope along each transect, weighted by the width of the confidence bands
width_ci_average	$0 \leq x \leq 0.19$	Average width of confidence band over the comprised transects
quality_flag	High/Medium/Low	Quality flag indicating the confidence in the slope estimate at this beach
mstr	$0.75\,m \leq x \leq 10\,m$	Mean Spring Tide Range at the beach calculated from the closest grid point in the FES2014 global tide model
hsig_median	$0.1\,m \leq x \leq 3\,m$	Median Significant Wave Height from the closest grid point in the CAWCR re-analysis dataset
prc_mstr_obs	$100\,\dfrac{\max(tide_{observed}) - \min(tide_{observed})}{MSTR}$	Percentage of the MSTR observed by the satellite-derived shorelines
min_tide_obs	$\min(tide_{observed})$	Lowest tide level observed by the satellite-derived shorelines
max_tide_obs	$\max(tide_{observed})$	Highest tide level observed by the satellite-derived shorelines
sl_points_average	$100 \leq x \leq 1300$	Average number of datapoints in the time-series over the comprised transects
beach_length	$75\,m \leq x \leq 50,000\,m$	Length of each beach or embayment. Very long beaches (> 50 km) were split to optimise memory as images are cropped around each beach
coastal_region	e.g., Southern NSW, Central Queensland, …	Database id corresponding to the 23 coastal regions as identified by Thom et al. (2018)

primary_comp_id	e.g., NSW01.01, NSW01.02, QLD01.01, …	Database id corresponding to the 100 primary sediment compartments as identified by Thom et al. (2018)
secondary_comp_id	e.g., NSW01.01.01, NSW01.01.02, QLD01.01.01, QLD01.01.02, …	Database id corresponding to the 361 secondary sediment Compartments as identified by Thom et al. (2018)

5 Discussion

This new beach-face slope dataset provides full coverage of the Australian sandy coast, with beach-face slope estimates for 132,000 transects spaced every 100 m and extending along 13,200 km of coast. By focusing on the beach-face slope (defined between MSL to MHWS), it complements an
240   existing dataset (Athanasiou et al., 2019) of nearshore slopes that are defined for the lower beach profile (between MSL and the depth of closure). While the nearshore slopes can be used to transform offshore wave parameters to the nearshore (see Figure 1), the beach-face slope is necessary to predict the elevation of wave run-up and total swash excursion at the shoreline that is used in most standard wave runup formulations (e.g., Stockdon et al., 2006). Consequently, this beach-face slope dataset is an important step towards improving predictions of wave run-up and potential inundation hazards along the Australian coast (O'Grady et al., 2019). Additionally, coastal flood warning systems (e.g., Doran et al., 2015; Leaman et al.,
245   2021; Stokes et al., 2019) often rely on a measure of the uncertainty associated with the input parameters to provide meaningful predictions with a margin of error. In that regard, the confidence bands associated with the beach-face slope estimates in this dataset can be used to propagate the uncertainty into the wave run-up equations and generate ensemble forecasts of total run-up elevation and swash excursion.

As identified in previous validation at 8 diverse sites (Vos et al., 2020), this dataset provides a good estimate of the 'typical' or long-term average beach-face slope obtained from 20 years of Landsat imagery. It is recognised however that the beach-face slope can vary quite substantially through
250   time, particularly for microtidal intermediate beaches (such as those found in SE Australia) where the beach often rapidly transitions between morphodynamic beach states (Wright and Short, 1984). While estimating this temporal variability is challenging using the described method on the historic Landsat data (as undertaken here), new satellite remote sensing capabilities may make this a future possibility. For example, by combining satellite missions such as Landsat, Sentinel-2 (5-days revisit at the equator) and Planet's CubeSat imagery (Kelly and Gontz, 2019), it might be possible to significantly increase the sampling frequency of shoreline observations. This higher-frequency data would enable a narrower time-
255   window in which beach-face slopes are estimated to be used, potentially opening up the possibility to estimate temporal variability in beach-face slopes at different timescales (e.g., inter-annual and seasonal).

While the focus of this dataset is on the Australian coastline, the generic nature of the method and global extent of Landsat imagery means that such a dataset could also be theoretically reproduced elsewhere. It is important to note however that the density of Landsat coverage is not consistent

globally (Wulder et al., 2016) and that Australia (along with North America and Eastern China) has some of the highest coverage in terms of image

260 density. Additionally, the Australian continent is characterised by a relatively low mean cloud frequency (Wilson and Jetz, 2016), which means that a lower proportion of optical images are hindered by clouds. Other areas with a sparser Landsat coverage and/or higher cloud frequency, may not have the same temporal depth of shoreline observations, which could hinder the applicability of this method in some regions.

5 Conclusion

This study presents a new dataset of beach-face slopes for the Australian coastline derived from a newly available remote sensing technique. The

265 dataset covers a total of 13,200 km of sandy coast and provides an estimate of the beach-face slope from Mean Sea Level (MSL) to Mean High Water Spring (MHWS) spaced every 100 m alongshore. Based on the width of the confidence bands around each slope estimate, it is found that 56% of the continental-scale dataset is classified as *high confidence*, while 23% have *medium confidence* and 21% have *low confidence*.

The dataset offers a unique view of large- to local-scale scale features in beach-face slope variability, providing data in regions with no *in situ* observational coverage. This new data availability opens up many interesting applications in coastal sciences and engineering, including:

270   i)   estimates (with confidence bands) of the beach-face slope parameter that is needed to predict wave run-up in coastal inundation forecasting systems (O'Grady et al., 2019);

    ii)   enhanced understanding of large-scale geologic factors contributing to the distribution of beach-face slopes and sediment grain sizes (Bujan et al., 2019; Short, 2020);

    iii)   informing coastal management and planning at the embayment scale;

275 The data is available in a simple format that can be readily imported into standard Geographical Information System software (e.g., QGIS, ArcGIS), or accessed programmatically, for use by coastal researchers and end-users.

Data Availability

The continental-scale beach-face slope dataset described in this manuscript (Section 3.3) is available in the following Zenodo data repository: https://doi.org/10.5281/zenodo.5606217 (Vos et al., 2021).

Code Availability

The source code to map satellite-derived shorelines from Landsat imagery (CoastSat) is available at https://doi.org/10.5281/zenodo.2779293 (Vos, 2021a). The source code to estimate beach-face slopes from satellite-derived shorelines and modelled tides (CoastSat.slope) is available at https://doi.org/10.5281/zenodo.3872442 (Vos, 2021b).

Acknowledgements

We acknowledge the great efforts by the United States Geological Survey / NASA for providing high-quality open-access data to the scientific community, Google Earth Engine for facilitating the access to the archive of publicly available satellite imagery, and CNES / LEGOS / CLS / AVISO for producing the global tide model FES2014, in particular Frederic Briol for developing the *fes* Python wrapper. Also thanks to the OpenStreetMap project and contributors (https://www.openstreetmap.org) for their extensive geospatial database. We also thank Nicolas Pucino for collecting and kindly sharing the grain size dataset along Stockton beach. We thank Floris Calkoen for his thorough review and constructive suggestions that greatly improved the final manuscript. The lead author is supported by a UNSW Scientia PhD scholarship.

Author Contribution

K.V., W.D., M.H.D., I.L.T. and K.D.S. devised the study, designed the figures, and wrote the manuscript. W.D. prepared the transect dataset and K.V. processed the beach-face slope data. All authors discussed the results and reviewed the manuscript.

Competing Interest

The authors declare that they have no conflict of interest.

References

Athanasiou, P., van Dongeren, A., Giardino, A., Vousdoukas, M., Gaytan-Aguilar, S. and Ranasinghe, R.: Global distribution of nearshore slopes with implications for coastal retreat, Earth Syst. Sci. Data Discuss., 11(4), 1–29, doi:10.5194/essd-2019-71, 2019.

Aucan, J., Hoeke, R. K., Storlazzi, C. D., Stopa, J., Wandres, M. and Lowe, R.: Waves do not contribute to global sea-level rise, Nat. Clim. Chang.,

9(1), 2–2, doi:10.1038/s41558-018-0377-5, 2019.

Bishop-Taylor, R., Sagar, S., Lymburner, L. and Beaman, R. J.: Between the tides: Modelling the elevation of Australia's exposed intertidal zone at continental scale, Estuar. Coast. Shelf Sci., 223(October 2018), 115–128, doi:10.1016/j.ecss.2019.03.006, 2019.

Bujan, N., Cox, R. and Masselink, G.: From fine sand to boulders: examining the relationship between beach-face slope and sediment size., Mar.
305 Geol., 106012, doi:10.1016/j.margeo.2019.106012, 2019.

Carrere, L., Lyard, F., Cancet, M., Guillot, A. and Picot, N.: FES 2014, a new tidal model—Validation results and perspectives for improvements, in Proceedings of the ESA living planet symposium, pp. 9–13., 2016.

Coastal Engineering Research Center: Shore protection manual, Dept. of the Army, Waterways Experiment Station, Corps of Engineers, Coastal Engineering Research Center. [online] Available from: https://books.google.com.au/books?id=km0YAQAAIAAJ, 1984.

310 Dean, R. G. and Dalrymple, R. A.: Coastal processes with engineering applications, Cambridge University Press., 2004.

Doran, K. S., Long, J. W. and Overbeck, J. R.: A method for determining average beach slope and beach slope variability for U.S. sandy coastlines., 2015.

Eleveld, M. A., Van der Wal, D. and Van Kessel, T.: Estuarine suspended particulate matter concentrations from sun-synchronous satellite remote sensing: Tidal and meteorological effects and biases, Remote Sens. Environ., 143, 204–215, doi:10.1016/j.rse.2013.12.019, 2014.

315 Gomes da Silva, P., Coco, G., Garnier, R. and Klein, A. H. F.: On the prediction of runup, setup and swash on beaches, Earth-Science Rev., 204, 103148, doi:10.1016/J.EARSCIREV.2020.103148, 2020.

GRASS Development Team: Geographic Resources Analysis Support System (GRASS GIS) Software, [online] Available from: https://grass.osgeo.org, 2020.

Greenslade, D., Hemer, M., Babanin, A., Lowe, R., Turner, I., Power, H., Young, I., Ierodiaconou, D., Hibbert, G., Williams, G., Aijaz, S.,
320 Albuquerque, J., Allen, S., Banner, M., Branson, P., Buchan, S., Burton, A., Bye, J., Cartwright, N., Chabchoub, A., Colberg, F., Contardo, S., Dufois, F., Earl-Spurr, C., Farr, D., Goodwin, I., Gunson, J., Hansen, J., Hanslow, D., Harley, M., Hetzel, Y., Hoeke, R., Jones, N., Kinsela, M., Liu, Q., Makarynskyy, O., Marcollo, H., Mazaheri, S., McConochie, J., Millar, G., Moltmann, T., Moodie, N., Morim, J., Morison, R., Orszaghova, J., Pattiaratchi, C., Pomeroy, A., Proctor, R., Provis, D., Reef, R., Rijnsdorp, D., Rutherford, M., Schulz, E., Shayer, J., Splinter, K., Steinberg, C., Strauss, D., Stuart, G., Symonds, G., Tarbath, K., Taylor, D., Taylor, J., Thotagamuwage, D., Toffoli, A., Valizadeh, A., Van Hazel, J., Da Silva,
325 G. V., Wandres, M., Whittaker, C., Williams, D., Winter, G., Xu, J., Zhong, A. and Zieger, S.: 15 priorities for wind-waves research: An Australian perspective, Bull. Am. Meteorol. Soc., 101(4), E446–E461, doi:10.1175/BAMS-D-18-0262.1, 2020.

Kelly, J. T. and Gontz, A. M.: Rapid Assessment of Shoreline Changes Induced by Tropical Cyclone Oma Using CubeSat Imagery in Southeast Queensland, Australia, J. Coast. Res., 36(1), 72, doi:10.2112/jcoastres-d-19-00055.1, 2019.

Leaman, C. K., Harley, M. D., Splinter, K. D., Thran, M. C., Kinsela, M. A. and Turner, I. L.: A storm hazard matrix combining coastal flooding
330   and beach erosion, Coast. Eng., 170, 104001, doi:10.1016/J.COASTALENG.2021.104001, 2021.

Lomb, N. R.: Least-squares frequency analysis of unequally spaced data, Astrophys. Space Sci., 39(2), 447–462, doi:10.1007/BF00648343, 1976.

Melet, A., Meyssignac, B., Almar, R. and Le Cozannet, G.: Under-estimated wave contribution to coastal sea-level rise, Nat. Clim. Chang., 8(3),
234–239, doi:10.1038/s41558-018-0088-y, 2018.

Middleton, J. H., Cooke, C. G., Kearney, E. T., Mumford, P. J., Mole, M. A., Nippard, G. J., Rizos, C., Splinter, K. D. and Turner, I. L.: Resolution
335   and accuracy of an airborne scanning laser system for beach surveys, J. Atmos. Ocean. Technol., 30(10), 2452–2464, doi:10.1175/JTECH-D-12-
00174.1, 2013.

O'Grady, J. G., McInnes, K. L., Hemer, M. A., Hoeke, R. K., Stephenson, A. G. and Colberg, F.: Extreme Water Levels for Australian Beaches
Using Empirical Equations for Shoreline Wave Setup, J. Geophys. Res. Ocean., 124(8), 5468–5484, doi:10.1029/2018jc014871, 2019.

OSM: OpenStreetMap contributers: Planet dump retrieved from https://planet.osm.org, 2017.

340   Pucino, N.: Coastal Dune Morphodynamic and Measures for Sand Stabilisation in Stockton Bight (NSW), University of Wollongong., 2015.

Pucino, N., Kennedy, D. M., Carvalho, R. C., Allan, B. and Ierodiaconou, D.: Citizen science for monitoring seasonal-scale beach erosion and
behaviour with aerial drones, Sci. Reports 2021 111, 11(1), 1–17, doi:10.1038/s41598-021-83477-6, 2021.

QGIS Development Team: QGIS Geographic Information System, [online] Available from: https://www.qgis.org, 2021.

Senechal, N., Coco, G., Bryan, K. R. and Holman, R. A.: Wave runup during extreme storm conditions, J. Geophys. Res. Ocean., 116(7), C07032,
345   doi:10.1029/2010JC006819, 2011.

Short, A. D.: Australian Coastal Systems, vol. 32, Springer International Publishing, Cham., 2020.

Short, A. D., Williamson, B. and Hogan, C. L.: The Australian Beach Safety and Management Program - Surf Life Saving Australia's Approach to
Beach Safety and Coastal Planning, 11th Australas. Conf. Coast. Ocean Eng. (Townsville, Qld.), National c(93/4), 113–118 [online] Available
from: https://search.informit.com.au/documentSummary;dn=560087890263399;res=IELENG, 1993.

350   Small, C., Nicholls, R. J., Summer, F. and Smallt, C.: A Global Analysis of Human Settlement in Coastal Zones, J. Coast. Res., 19(3), 584–599,
doi:10.2307/4299200, 2011.

Stephens, S. A., Coco, G. and Bryan, K. R.: Numerical Simulations of Wave Setup over Barred Beach Profiles: Implications for Predictability, J.
Waterw. Port, Coast. Ocean Eng., 137(4), 175–181, doi:10.1061/(ASCE)WW.1943-5460.0000076, 2011.

Stockdon, H. F., Asbury H., Jr., S., List, J. H. and Holman, R. A.: Estimation of Shoreline Position and Change Using Airborne Topographic Lidar
355   Data, J. Coast. Res., 18(3), 502–513, doi:10.2307/4299097, 2002.

Stockdon, H. F., Holman, R. A., Howd, P. A. and Sallenger, A. H.: Empirical parameterization of setup, swash, and runup, Coast. Eng., 53(7), 573–

588, doi:10.1016/j.coastaleng.2005.12.005, 2006.

Stockdon, H. F., Sallenger, A. H., Holman, R. A. and Howd, P. A.: A simple model for the spatially-variable coastal response to hurricanes, Mar. Geol., 238(14), 1–20, doi:10.1016/j.margeo.2006.11.004, 2007.

360   Stokes, K., Poate, T. and Masselink, G.: Development of a real-time, regional coastal flood warning system for southwest England, in Coastal Sediments 2019, pp. 1460–1474, World Scientific Pub Co Pte Lt., 2019.

Thom, B. G., Eliot, I., Eliot, M., Harvey, N., Rissik, D., Sharples, C., Short, A. D. and Woodroffe, C. D.: National sediment compartment framework for Australian coastal management, Ocean Coast. Manag., 154(July 2017), 103–120, doi:10.1016/j.ocecoaman.2018.01.001, 2018.

Tseng, K. H., Kuo, C. Y., Lin, T. H., Huang, Z. C., Lin, Y. C., Liao, W. H. and Chen, C. F.: Reconstruction of time-varying tidal flat topography

365   using optical remote sensing imageries, ISPRS J. Photogramm. Remote Sens., 131, 92–103, doi:10.1016/j.isprsjprs.2017.07.008, 2017.

Turner, I. L., Harley, M. D. and Drummond, C. D.: UAVs for coastal surveying, Coast. Eng., 114, 19–24, doi:10.1016/j.coastaleng.2016.03.011, 2016.

VanderPlas, J. T.: Understanding the Lomb–Scargle Periodogram, Astrophys. J. Suppl. Ser., 236(1), 16, doi:10.3847/1538-4365/aab766, 2018.

Vitousek, S., Barnard, P. L., Fletcher, C. H., Frazer, N., Erikson, L. and Storlazzi, C. D.: Doubling of coastal flooding frequency within decades

370   due to sea-level rise, Sci. Rep., 7(1), 1–9, doi:10.1038/s41598-017-01362-7, 2017.

Vos, K.: kvos/CoastSat: CoastSat v1.1.1, , doi:10.5281/ZENODO.4649450, 2021a.

Vos, K.: kvos/CoastSat.slope: CoastSat.slope v1.0.2, , doi:10.5281/ZENODO.5372830, 2021b.

Vos, K., Splinter, K. D., Harley, M. D., Simmons, J. A. and Turner, I. L.: CoastSat: A Google Earth Engine-enabled Python toolkit to extract shorelines from publicly available satellite imagery, Environ. Model. Softw., 122, 104528, doi:10.1016/j.envsoft.2019.104528, 2019a.

375   Vos, K., Harley, M. D., Splinter, K. D., Simmons, J. A. and Turner, I. L.: Sub-annual to multi-decadal shoreline variability from publicly available satellite imagery, Coast. Eng., 150, 160–174, doi:10.1016/j.coastaleng.2019.04.004, 2019b.

Vos, K., Harley, M. D., Splinter, K. D., Walker, A. and Turner, I. L.: Beach Slopes From Satellite-Derived Shorelines, Geophys. Res. Lett., 47(14), doi:10.1029/2020GL088365, 2020.

Vos, K., Harley, M. D., Splinter, K. D., Turner, I. L. and Wen, D.: Beach-face slope dataset for Australia, , doi:10.5281/ZENODO.5606217, 2021.

380   Wilson, A. M. and Jetz, W.: Remotely Sensed High-Resolution Global Cloud Dynamics for Predicting Ecosystem and Biodiversity Distributions, PLoS Biol, 14(3), 1002415, doi:10.1371/journal.pbio.1002415, 2016.

Wright, L. D. and Short, A. D.: Morphodynamic variability of surf zones and beaches: A synthesis, Mar. Geol., 56(1–4), 93–118, doi:10.1016/0025-3227(84)90008-2, 1984.

Wulder, M. A., White, J. C., Loveland, T. R., Woodcock, C. E., Belward, A. S., Cohen, W. B., Fosnight, E. A., Shaw, J., Masek, J. G. and Roy, D.

385   P.: The global Landsat archive: Status, consolidation, and direction, Remote Sens. Environ., 185, 271–283, doi:10.1016/j.rse.2015.11.032, 2016.